PHYSICAL REVIEW B VOLUME 27, NUMBER 12 15 JUNE 1983

Effects of impurity-band tails on Auger recombination in semiconductors

Masumi Takeshima
Semiconductor Laboratory, Matsushita Electronics Corporation, Takatsuki, Osaka, Japan
(Received 10 December 1982)

The impurity-assisted Auger recombination rates in highly doped semiconductors are calculated on the basis of the semiempirical pseudopotential method, which has recently been developed for the Green's-function analysis of the impurity-band tails. The calculation is an alternative to the previously reported calculation based on the Green's function derived by Bonch-Bruevich, which well describes only the intraband states far from the tail ones at high doping levels. It is shown that the effect of the tail states on the Auger recombination is important only at low temperatures in GaAs and InP, the band-gap energy of which is much larger than the spin split-off energy, and over a wide temperature range in GaSb and InAs, for which both energies are comparable.

I. INTRODUCTION

The Auger recombination (AR) of excess carriers offers an essential energy-loss mechanism in excited semiconductors under high carrier concentrations. The fundamental Auger process is the pure-collision Auger recombination (PCAR), about which extensive literature[1] has been published ever since the successful work by Beatie and Landsberg.[2] Although the PCAR analysis is prevailing owing considerably to the mathematical tractability, it has become clear that the analysis alone is insufficient to explain various experiments.[3–7] In order to give a better explanation the phonon-assisted Auger recombination[8] and the impurity-assisted Auger recombination[9] (IAAR), i.e., AR assisted by the ionized impurity scattering, have been proposed.

A method for a comprehensive understanding of AR assisted by various scatterings has been given[10] by this author on the basis of the Green's-function formalism. Into the Green's-function scattering effects can be incorporated. In a special case of no scattering effects PCAR can be obtained. Another merit of the method is that the well-known difficulty of divergence, which is inherent in the second-order perturbation treatment,[11] is avoided.[12]

In an attempt to understand AR over a wide doping range, the present author has given a unified theory of the impurity and phonon scattering effects on the recombination in a previous paper[13] (referred to as I). There, use was made of the Green's function which had been derived by Bonch-Bruevich[14] for the impurity scattering problem and was modified by the present author to take into account the phonon scattering effect. Hereafter we call this scattering theory the BT theory. The BT theory is useful at high doping levels for description of the perturbed intraband states far from the tail ones but gives a poor description of the tail states. In fact, calculated density of the tail states is found[15] to be much smaller than the experimental ones. In I, therefore, the effect of the impurity-band tails is small and has been practically neglected in calculating the quasi-Fermi levels.

As an alternative to the BT theory, the present author has developed the semiempirical pseudopotential theory[15] for calculating the Green's function. Hereafter we call this theory the ps theory. The theory is based on replacing the true potentials in the BT theory by the pseudopotentials which are contrived as effective potentials due to randomly distributed impurities. It was found that the ps theory gives a satisfactory description of the tail states experimentally observed. The number of the tail states is so large that considerably many of the carriers are in these states. Therefore, it is not appropriate to neglect the tail states in calculating the Fermi level, as has been done in I.

The purpose of this paper is to present calculations of the IAAR rates based on the Green's function in the ps theory. Calculations are done for p-type materials of GaAs, InP, GaSb, and InAs, which have direct band gaps. These are typical in that we have $E_G \gg \Delta_0$ for the former two materials and $E_G \simeq \Delta_0$ for the latter two, where E_G and Δ_0 are the band-gap and the spin-splitoff energies, respectively. Experimental data are available for p-type GaAs and p-type GaSb for comparison. As for p-type GaSb, the calculation in I shows[16] a marked deviation from the experiments especially at acceptor concentrations exceeding about 1×10^{19} cm^{-3}. This is a direct impetus for the present work and the ex-

 ©1983 The American Physical Society

periments are qualitatively explained by the present theory.

II. THEORY

An expression for the AR lifetime of excess carriers is given[10] in terms of the retarded Green's function $G^R(l,\vec{k};\omega)$ at an energy ω for a band l with a wave vector $\vec{k}$. That the Green's function is given for a specified band comes from neglecting interband scattering effects. It is assumed that the conduction-band (CB) electrons and the valence-band (VB) electrons belong to two different systems, each of which is in thermal equilibrium within itself and with the phonon system. Thus the CB and the VB systems are describable by quasi-Fermi levels μ_c and μ_v, respectively, and by one temperature. The expression for the excess carrier lifetime τ is given by

$$\frac{1}{\tau}=\frac{4}{n_C\hbar\pi^3}\int\frac{d\vec{k}_2}{(2\pi)^3}\int\frac{d\vec{k}_3}{(2\pi)^3}\int\frac{d\vec{k}_4}{(2\pi)^3}(|f|^2+|g|^2+|f-g|^2)$$
$$\times\int d\omega_1\int d\omega_2\int d\omega_3\int d\omega_4\Theta_{\rm IF}\delta(\omega_{\rm IF})\prod_{i=1}^{4}{\rm Im}G^R(l_i,\vec{k}_i;\omega_i)\ . \tag{2.1}$$

Here ω_i is measured from the quasi-Fermi level relevant to the band l_i. We define $\vec{k}_1=\vec{k}_3+\vec{k}_4-\vec{k}_2$. $\Theta_{\rm IF}$ is the statistical factor given in terms of the Fermi-Dirac distribution function $\theta_i=\theta(\omega_i)$, i.e.,

$$\theta_i=\frac{1}{\exp\left[\frac{\omega_i}{T}\right]+1}\ , \tag{2.2}$$

as

$$\Theta_{\rm IF}=(1-\theta_1)(1-\theta_2)\theta_3\theta_4 -\theta_1\theta_2(1-\theta_3)(1-\theta_4) \tag{2.3}$$

for the initial (I) and the final (F) states: Here T is the thermal energy. $\omega_{\rm IF}$ is the energy difference,

$$\omega_{\rm IF}=\omega_1+\omega_2-\omega_3-\omega_4-\mu_c+\mu_v\ , \tag{2.4}$$

for the initial and the final states. n_C is the excess carrier concentration. We define

$$f=\langle l_1,\vec{k}_1\,|\,l_4,\vec{k}_4\rangle\langle l_2,\vec{k}_2\,|\,l_3,\vec{k}_3\rangle U(\vec{k}_4-\vec{k}_1)\ ,$$
$$g=\langle l_1,\vec{k}_1\,|\,l_3,\vec{k}_3\rangle\langle l_2,\vec{k}_2\,|\,l_4,\vec{k}_4\rangle U(\vec{k}_3-\vec{k}_1)\ , \tag{2.5}$$

where $\langle l_i,\vec{k}_i\,|\,l_j,\vec{k}_j\rangle$ is the overlap integral between the modulating parts of the Bloch functions $|\,l_i,\vec{k}_i\rangle$ and $|\,l_j,\vec{k}_j\rangle$, which are normalized over the crystal volume. $U(\vec{k})$ is the Fourier component of the electron-electron screened Coulomb interaction times the crystal volume, i.e.,

$$U(\vec{k})=\frac{4\pi e^2}{\epsilon_0}\frac{1}{k^2+\lambda^2}\ , \tag{2.6}$$

where e is the electronic charge, ϵ_0 the static dielectric constant of the host lattice, and λ the inverse screening length discussed later. f and g represent the Coulomb term and the exchange term, respectively. We consider the screening for both terms equally on the basis of discussions given.[16] Each Green's function in Eq. (2.1) should be understood to be given[9,13] after taking an ensemble average over all the impurity sites.

Let us restrict the discussion to p-type materials containing singly ionized shallow acceptors of concentration n_i. We consider the Auger transition among CB, the heavy-hole band (HB), and the spin-splitoff band (SB), as shown in Fig. 1. The process where SB is replaced by the light-hole band is important only for materials with $\Delta_0\gg E_G$, which are not considered here. Figure 1(a) shows PCAR. In the presence of the impurity scattering, intermediate states can intervene between the states 4 and 1 and between 3 and 2. Noting that scattering effects are important for a heavy-mass band, we consider the impurity scattering effect for HB only and neglect the effect for CB and SB. This facilitates the calculation for Eq. (2.1) through

$${\rm Im}G^R(l_i,\vec{k}_i;\omega_i)={\rm Im}G_0^R(l_i,\vec{k}_i;\omega_i)=-\pi\delta(\omega_i-\xi_i)$$

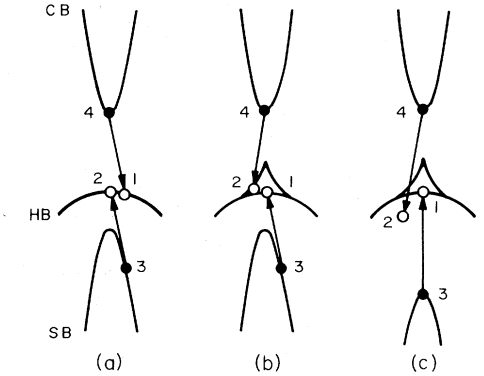

FIG. 1. (a) AR processes among CB, HB, and SB for PCAR, (b) for IAAR with $E_G\gg\Delta_0$, and (c) for IAAR with $E_G<\Delta_0$.

for $i=3,4$. Here $G_0^R(l_i,\vec{k}_i;\omega_i)$ is the free-particle Green's function, δ is Dirac's δ function, and $\xi_i=\xi_{l_i\vec{k}_i}$ is the unperturbed band energy for a state $l_i,\vec{k}_i$ which is measured from the relevant quasi-Fermi level.

Now we must give the Green's function for HB, i.e., for $i=1,2$ in Eq. (2.1). In the ps theory the Green's function is given as

$$G^R(l_H,\vec{k};\omega)=\frac{\epsilon_0}{e^2\lambda}\bar{G}^R(\Omega)\ , \tag{2.7}$$

where l_H denote HB and we define

$$\Omega=\frac{\epsilon_0}{e^2\lambda}(\omega-\xi_{l_H\vec{k}})\ . \tag{2.8}$$

Thus the dependence of G^R on ω and $\xi_{l_H\vec{k}}$ is given through a single parameter Ω. Using a cutoff value Ω_c given later, we give $\mathrm{Im}\bar{G}^R(\Omega)=0$ in the range $\Omega>\Omega_c$. We need not know $\mathrm{Re}\bar{G}^R(\Omega)$ in the present calculation. In the range $\Omega\le\Omega_c$ we have

$$\bar{G}^R(\Omega)=\frac{1}{i}\int_0^\infty d\xi\exp[i\xi\Omega+\gamma g(\xi)]\ , \tag{2.9}$$

$$g(\xi)=\int_0^\infty dx\,x^2\{\exp[-i\xi h^{\mathrm{PS}}(x)] +i\xi h(x)-1\}\ , \tag{2.10}$$

$$h^{\mathrm{PS}}(x)=h(x)+h^r(x)\ , \tag{2.11}$$

$$h(x)=\frac{1}{x}\exp(-x)\ , \tag{2.12}$$

$$h^r(x)=-\frac{1}{2}\frac{a_B\lambda}{(x+x_0)^2}\times\left[2(1+x)^2-\exp\left[-\frac{x}{x_0}\right]\right]\times\exp\left[-\frac{2x^2}{x+x_0}\right]\ , \tag{2.13}$$

$$\gamma=\frac{4\pi n_i}{\lambda^3}\ , \tag{2.14}$$

where $x_0=\lambda[3/(4\pi n_i)]^{1/3}$ and $a_B=\hbar^2\epsilon_0/(m_He^2)$: m_H is the effective mass for HB whose energy surface is assumed to be spherical. If we consider some other band, m_H in a_B should be replaced by the relevant mass. It is to be noted that we have $\mathrm{Im}\bar{G}^R(\Omega)=0$ in the range $\Omega<-\gamma$ as a general consequence of the ps theory as well as the BT theory.[13] The criterion under which the ps theory is useful has been given.[15] According to the criterion the theory is useful for HB but not for CB and SB in the present case of a p-type material having direct band gap.

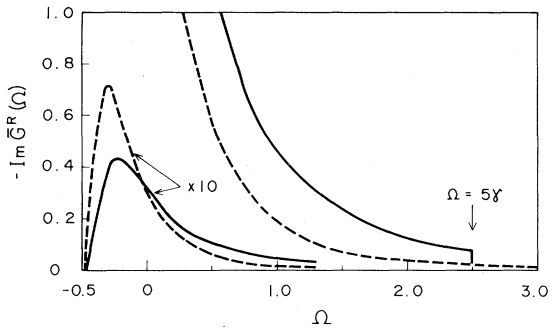

FIG. 2. $\mathrm{Im}\bar{G}^R(\Omega)$ vs Ω in the ps theory (solid line) and in the BT theory (dashed line) for $\gamma=0.5$ and $a_B\lambda=0.57$. An arrow shows a cutoff at $\Omega=\Omega_c\equiv5\gamma$.

Especially when we take $h^r(x)=0$ and $\Omega_c\to\infty$, Eqs. (2.7)–(2.14) are the expressions in the BT theory. In this theory the impurity potential is assumed to vary so slowly that the fluctuations in the energy of the electronic states mirror closely those in the potential energy. The assumption is the semiclassical one and is rigorous when $a_B=0$ giving $h^r(x)=0$. Thus the quantum effect is incorporated into the theory in terms of $h^r(x)$. Since $h(x)$ is the normalized potential due to any one of impurities of one species, $h^{\mathrm{PS}}(x)=h(x)+h^r(x)$ is the effective potential including the quantum correction. Therefore $h^{\mathrm{PS}}(x)$ was called in Ref. 15 the pseudopotential after the conventional pseudopotentials, although these have nothing in common with the present context. In the BT theory $\bar{G}^R(\Omega)$ is independent of the relevant band parameters. Therefore the Green's functions in Eq. (2.1) are treated in I on an equal footing for all bands. In contrast, the scattering effects are taken into account only for HB in the present paper, considering that the effects are dominant in the heavy-mass band. This is one of the marked differences from the treatments in I.

Figure 2 shows an example of the calculated curves of $\mathrm{Im}\bar{G}^R(\Omega)$ in the ps theory (solid line) and in the BT theory (dashed line). In accordance with Ref. 15, we take $\Omega_c=5\gamma$ hereafter. To find the quasi-Fermi level for VB, we calculate the energy density of states $\rho(\omega)$ for HB from

$$\rho(\omega)=-\frac{2}{\pi}\int\frac{d\vec{k}}{(2\pi)^3}\mathrm{Im}G^R(l_H,\vec{k};\omega)\ , \tag{2.15}$$

neglecting the contribution from the light-hole band. In the limit of $\omega\to-\infty$, $\rho(\omega)$ should agree with the value for the unperturbed band. This requirement leads to

$$\int_{-\infty}^{\infty}d\Omega\,\mathrm{Im}\bar{G}^R(\Omega)=-\pi\ . \tag{2.16}$$

This is found with the use of Eq. (2.9) under the assumption of $\Omega_c \to \infty$. In the ps theory a sharp cutoff of $\mathrm{Im}\bar{G}^R(\Omega)$ at $\Omega=\Omega_c$ is only an approximation and gives a value of the integral smaller in magnitude than π although the error may be small. The quasi-Fermi level for VB is calculated using

$$n_i = \int_{-\infty}^{\infty} d\omega \rho(\omega)\theta(\omega) . \tag{2.17}$$

Owing to a long band tail found from the relation, the quasi-Fermi level is appreciably pulled toward the mid-gap state. This is another of the marked differences from the treatments in I, where the quasi-Fermi level is calculated neglecting the tail states.

Let us consider the inverse screening length, which is given[13] under the Thomas-Fermi approach by

$$\lambda^2 = \frac{16e^2}{\epsilon_0} \lim_{\vec{q}\to 0} \int_{-\infty}^{\infty} d\omega\, \theta(\omega) \int \frac{d\vec{k}}{(2\pi)^3} \mathrm{Im}G^R(l_H,\vec{k};\omega)[\mathrm{Re}G^R(l_H,\vec{k}+\vec{q};\omega)+\mathrm{Re}G^R(l_H,\vec{k}-\vec{q};\omega)] , \tag{2.18}$$

neglecting the screening delay, i.e., the ω dependence of the screening. It is to be noted that the above expression never reduces to a form

$$\lambda^2 = -\frac{4\pi e^2}{\epsilon_0} \int_{-\infty}^{\infty} d\omega \rho(\omega) \frac{\partial}{\partial\omega}\theta(\omega) , \tag{2.19}$$

which has been adopted by Hwang.[17] Instead, by expanding $\theta(\omega)$ as

$$\theta(\omega) = \sum_{n=0}^{\infty} \frac{1}{n!}(\omega-\xi_{l_H\vec{k}})^n \frac{\partial^n}{\partial\xi_{l_H\vec{k}}^n}\theta(\xi_{l_H\vec{k}}) , \tag{2.20}$$

and taking approximately $\Omega_c \to \infty$, we obtain[13] for $\vec{q}\to 0$,

$$\lambda^2 = -\frac{8\pi e^2}{\epsilon_0} \int \frac{d\vec{k}}{(2\pi)^3} \frac{\partial}{\partial\xi_{l_H\vec{k}}}\theta(\xi_{l_H\vec{k}}) . \tag{2.21}$$

In the same approach we obtain

$$n_i = 2\int \frac{d\vec{k}}{(2\pi)^3}\theta(\xi_{l_H\vec{k}}) . \tag{2.22}$$

The expression (2.21) can be rewritten in the form of Eq. (2.19), taking $\rho(\omega)$ to be the density of states for the unperturbed band.

The expansion given by Eq. (2.20) is useful when the energy width of $\mathrm{Im}\bar{G}^R(\Omega)$ is much smaller than the thermal energy, i.e.,

$$T \gg \frac{e^2\lambda}{\epsilon_0}\gamma .$$

On the other hand, the approximation $\Omega_c \to \infty$ is not too inaccurate since contributions of $\mathrm{Im}\bar{G}^R(\Omega)$ from the range $\Omega > 5\gamma$ are small. For a general calculation of λ we must solve Eqs. (2.7), (2.15), (2.17), and (2.18) consistently, but this is time-consuming work. In place of doing this, we determine λ from Eqs. (2.21) and (2.22) although this may be only approximately valid. This procedure has been adopted also in I. On the other hand, the quasi-Fermi level for VB should be determined from Eqs. (2.15) and (2.17) in order to give Θ_{IF} in Eq. (2.1).

Now we put Eq. (2.1) into more tractable form. Let nondegenerate statistics be assumed for excess carriers in CB. We have $n_C = N_c \exp\eta_n$, where $T\eta_n$ is the quasi-Fermi level for CB measured upward from the CB edge and N_C the effective density of states for CB given by

$$N_C = 2[m_C T/(2\pi\hbar^2)]^{3/2} .$$

m_C is the effective mass for CB. We make approximations

$$\prod_{i=1}^{4} \mathrm{Im}G^R(i) = \mathrm{Im}G^R(1)\mathrm{Im}G^R(2)\mathrm{Im}G_0^R(3)\mathrm{Im}G_0^R(4), \quad \theta_3 = 1$$

giving $\Theta_{\mathrm{IF}} = (1-\theta_1)(1-\theta_2)\theta_4$, and

$$|f|^2+|g|^2+|f-g|^2 = \left[\frac{2\pi e^2\hbar^2}{m_0\epsilon_0 E_G}\right]^2 f_{\mathrm{CH}} f_{\mathrm{SH}} \left[\left[\frac{|\vec{k}_1-\vec{k}_3|^2}{|\vec{k}_1-\vec{k}_3|^2+\lambda^2}\right]^2 + \left[\frac{|\vec{k}_2-\vec{k}_3|^2}{|\vec{k}_2-\vec{k}_3|^2+\lambda^2}\right]^2\right] , \tag{2.23}$$

where $G^R(i) = G^R(l_i\vec{k}_i,\omega_i)$, f_{CH} and f_{SH} are the oscillator strengths between CB and HB and between SB and

HB, respectively, and m_0 is the electron mass in the free space. We define the energy E_i for a band l_i, which is measured from the relevant band edge so as to be positive. Assuming spherical energy surfaces for all bands we have $E_1=\hbar^2k_1^2/(2m_H)$, $E_2=\hbar^2k_2^2/(2m_H)$, $E_3=\hbar^2k_3^2/(2m_S)$, and $E_4=\hbar^2k_4^2/(2m_C)$, where m_S is the effective mass for SB. After some manipulations we obtain

$$\frac{1}{\tau}=\frac{8T^2(m_Sm_H)^{3/2}e^4}{\pi^{7/2}\hbar^3(\epsilon_0m_0E_G)^2\xi_\lambda}f_{\rm CH}\exp(2\eta_p+z_0-z_1)\int_{-z_1}^{\infty}dz\,(z+z_1)^{1/2}\exp(-z)f_{\rm SH}S(z)\ , \tag{2.24}$$

where

$$S(z)=\int_0^\infty dr\,r^5\int_0^1 d\phi\,\phi^2(1-\phi^2)^{1/2}\int_{-1}^1 d\phi_1\int_{-1}^1 d\phi_2(\Psi_{13}+\Psi_{23})$$
$$\times\int_{-\gamma}^{\Omega_c}d\Omega\,{\rm Im}\bar{G}^R(\Omega){\rm Im}\bar{G}^R(\Omega_0-\Omega)\frac{1}{1+\exp(\eta_p+\xi_\lambda\Omega_1)}\frac{1}{1+\exp(\eta_p+\xi_\lambda\Omega_2)}\ . \tag{2.25}$$

We define $T\eta_p$ as the quasi-Fermi level for VB measured downward from the VB edge, $z_0=(E_G-\Delta_0)/T$, $z_1=(z_0+|z_0|)/2$, $\xi_\lambda=e^2\lambda/(\epsilon_0T)$, $\eta_i=E_i/T$ $(i=1,2,3,4)$, $\Omega_0=(\eta_1+\gamma^2-z-z_1+z_0)/\xi_\lambda$, $\Omega_1=\Omega-\eta_1/\xi_\lambda$, and $\Omega_2=\Omega_0-\Omega-\eta_2/\xi_\lambda$. We also define $\sqrt{\eta_4}=r\phi$, $\sqrt{\eta_2}=r(1-\phi^2)^{1/2}$, $\vec{k}_2\cdot\vec{k}_3/(k_2k_3)=\phi_1$, $(\vec{k}_3-\vec{k}_2)\cdot\vec{k}_4/(|\vec{k}_3-\vec{k}_2|k_4)=\phi_2$. Ψ_{13} and Ψ_{23} are the first term and the second term, respectively, in the square brackets in Eq. (2.23). Ψ_{13} is given approximately by taking an average over the angle between $\vec{k}_1$ and $\vec{k}_3$. We have

$$\Psi_{13}=1+\frac{\eta_\lambda^2}{(\eta_1+\eta_3+\eta_\lambda)^2-4\eta_1\eta_3}-\frac{\eta_\lambda}{2\sqrt{\eta_1\eta_3}}\ln\left|\frac{(\sqrt{\eta_1}+\sqrt{\eta_3})^2+\eta_\lambda}{(\sqrt{\eta_1}-\sqrt{\eta_3})^2+\eta_\lambda}\right|$$

and

$$\Psi_{23}=\left[\frac{\eta_2+\eta_3-2\phi_1\sqrt{\eta_2\eta_3}}{\eta_2+\eta_3-2\phi_1\sqrt{\eta_2\eta_3}+\eta_\lambda}\right]^2,$$

where $\eta_\lambda=\hbar^2\lambda^2/(2m_HT)$. η_3 and η_1 are expressed as $\eta_3=(z+z_1)m_S/m_H$ and

$$\eta_1=\mu_H(r\phi)^2+2\phi_2[\mu_Hr\phi(\eta_2+\eta_3-2\phi_1\sqrt{\eta_2\eta_3})]^{1/2}+\eta_2+\eta_3-2\phi_1\sqrt{\eta_2\eta_3}\ ,$$

with $\mu_H=m_C/m_H$. $f_{\rm CH}$ and m_S are evaluated for the threshold condition, which is generally found in the second-order perturbation treatment.[18] This is done also for $f_{\rm SH}$ if $E_G-\Delta_0\gg\Delta_0$ but we use $f_{\rm SH}=f'_{\rm SH}E_2$ with $f'_{\rm SH}=df_{\rm SH}/dE_2$ at $E_2=0$ when $-\infty<E_G-\Delta_0\ll\Delta_0$. The former is the case for GaAs and InP while the latter is the case of GaSb and InAs.

In a practical calculation of $S(z)$ a range for the integration over r can be restricted to be more nar-

TABLE I. Material parameters and band parameters.

Parameter	GaAs	InP	GaSb	InAs
E_{G0} (eV)	1.522	1.421	0.8128	0.4105
Δ_{00} (eV)	0.34	0.13	0.743	0.38
E_{G1} (eV K^{-1})	5.8×10^{-4}	2.9×10^{-4}	3.7×10^{-4}	3.35×10^{-4}
Δ_{01} (eV K^{-1})	0	0	1.89×10^{-4}	1.0×10^{-4}
T_0 (K)	300	0	0	248
m_C/m_0[c]	0.067	0.078	0.043	0.023
m_H/m_0	0.45	0.65[b]	0.33	0.41
m_S/m_0[c]	0.11	0.12	0.12	0.083
$f_{\rm CH}$[c]	2.25–2.60[d]	1.82–2.02[d]	9.64	18.0
$f_{\rm SH}$[c]	1.99	1.84	$4.34E_2$[a]	$20.1E_2$[a]
ϵ_0	13.18	12.35	15.69	14.55

[a] E_2 in eV.
[b] Assumed.
[c] Calculated.
[d] In the range from 77 to 500 K.

row. The condition where a product $\mathrm{Im}\bar{G}^R(\Omega)\mathrm{Im}\bar{G}^R(\Omega_0-\Omega)$ is different from zero is given by $-\gamma\leq\Omega\leq\Omega_c$ and $-\gamma\leq\Omega_0-\Omega\leq\Omega_c$. These inequalities give an upper bound of the integration as $r=r_m$ in place of infinity, where $r_m=(z+z_1-z_0+2\xi_\lambda\Omega_c)^{1/2}$. Computation of $S(z)$ using Weyl's Gleichverteilung method followed by numerical integration over z is performed. At least 500 combinations of $(r,\phi,\phi_1,\phi_2,\Omega)$ with random values are found to yield well convergent results.

III. RESULTS AND DISCUSSIONS

The theory in the preceding section is applied to p-type materials of GaAs, InP, GaSb, and InAs, which contain single ionized acceptors. We take into account the temperature dependence of E_G and Δ_0, giving

$$E_G=E_{G0}-E_{G1}T^2/(T+T_0) \tag{3.1}$$

and

$$\Delta_0=\Delta_{00}+\Delta_{01}T\ , \tag{3.2}$$

where E_{G0}, E_{G1}, Δ_{01}, and T_0 are material parameters. Some of the band parameters to be used are found from Ref. 19 and the others are calculated on the basis of the $\vec{k}\cdot\vec{p}$ perturbation theory[20] using the numerical values of the interband matrix elements given by Lawaetz.[21]

The material parameters and the band parameters are shown in Table I. It is to be noted that the values of m_H for InP and of f_{CH} for GaAs and InP are different from those used in I. As for m_H/m_0 for InP, the value 0.8 used in I seems to be too large and the value 0.65 is assumed.[22] As for f_{CH}, it has been pointed out[16] that the conventional evaluation, which has been adopted in I, is not appropriate. The improved calculation is required especially for GaAs and InP which have $E_G-\Delta_0\gg\Delta_0$. Taking into account the temperature dependence, f_{CH}'s are given in the temperature range from 77 to 500 K. These values are considerably smaller than those given in I, i.e., $f_{\mathrm{CH}}=5.63$ and 4.76 for GaAs and InP, respectively.

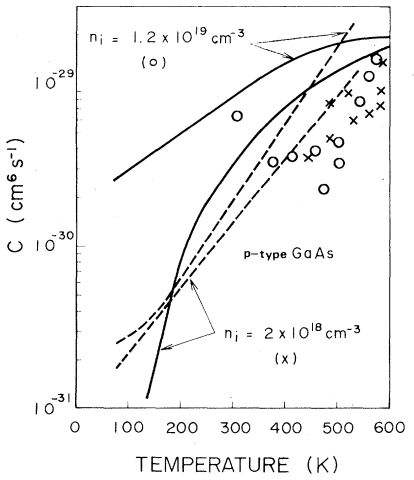

FIG. 3. Auger coefficients C vs temperature at $n_i=2\times10^{18}$ cm^{-3} and 1.2×10^{19} cm^{-3} on p-type GaAs for the ps results (solid line), for the BT results (dashed line), and for the experimental results (open circles and crosses).

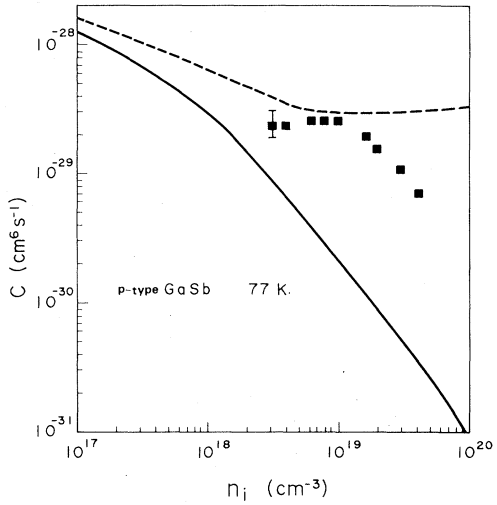

FIG. 4. Auger coefficients C vs n_i at 77 K on p-type GaSb for the ps result (solid line), for the BT result (dashed line), and for the experimental results (filled squares).

Now we present results of τ in terms of the Auger coefficient C defined through $\tau^{-1}=Cn_i^2$. It is to be noted that in I the Auger coefficient $\pi^{-1}C$ is defined through $\tau^{-1}=\pi^{-1}Cn_i^2$. Let us call the present results and those in I the ps results and the BT results, respectively. For the purpose of comparison the BT results are shown on the basis of the present definition of C, making necessary corrections of f_{CH}. Under the ps models we neglect the phonon scattering effects, which are found to be smaller than the impurity scattering effects over almost all of the range of n_i considered.

Figure 3 shows the ps results (solid line), the BT results (dashed line), and the experimental results (open circles and crosses) on p-type GaAs as functions of temperature for two values of n_i. It is seen that the ps results and the BT results are close at high temperatures, where the experimental data are available.[23] The points are calculated from the data of the excess carrier lifetime. In presenting these data and in evaluating the Auger lifetime, some assumptions which are not so well established are used

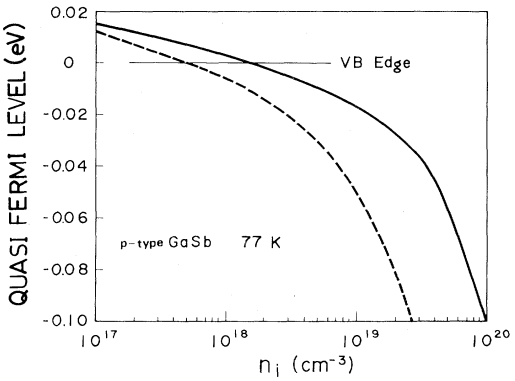

FIG. 5. Quasi-Fermi levels for VB on p-GaSb at 77 K based on the ps model (solid line) and on the unperturbed band model (dashed line), which are measured from the unperturbed VB edge.

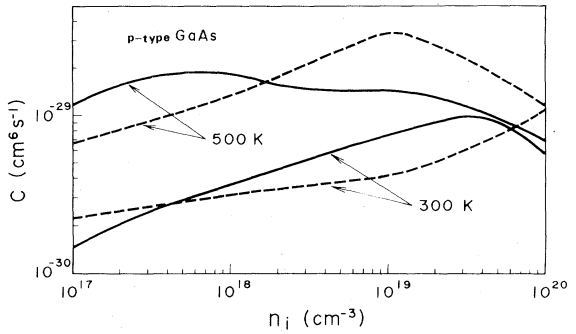

FIG. 6. Auger coefficients C vs n_i at 300 and 500 K on p-type GaAs for the ps results (solid line) and for the BT result (dashed line).

so that considerable errors should be included. In view of this, agreement between the theories and the experiments is fairly good. At low temperatures the dependence of C on n_i is larger for the ps results than for the BT results. Even a sharp cutoff of C is seen at a temperature for a smaller n_i in the ps results. This cutoff results from a sharp cutoff of $\mathrm{Im}\bar{G}^R(\Omega)$ at $\Omega=\Omega_c$. Thus the marked increase of C with increasing n_i results from increase of the width of $\mathrm{Im}\bar{G}^R(\Omega)$, i.e., of the number of the tail states.

Figure 4 shows the ps result (solid line), the BT result (dashed line), and the experimental results (filled squares) on p-GaSb as functions of n_i. The experimental points are calculated from the data[24] of the Auger lifetime. The ps result and the BT result are fairly close at $n_i \lesssim 10^{18}$ cm^{-3}, showing rather slow variations of C's with n_i. At larger n_i's, on the other hand, the ps result showing rapidly varying C is in remarkable contrast to the BT result showing nearly constant C. Thus the ps result shows the curve which considerably simulates the experimental plots though the plots lie in between two curves. The rapid decrease of C with increasing n_i in the ps result comes from increase of the width of $\mathrm{Im}\bar{G}^R(\Omega)$, i.e., of the number of the tail states.

The remarkable contrast found between GaAs and GaSb in the ps results is discussed. First it is to be noted that the role of the tail states is to elevate the quasi-Fermi level for VB above the value calculated for the unperturbed band. This is shown in Fig. 5, where the quasi-Fermi levels are calculated on the ps model (solid line) and on the unperturbed band model (dashed line) for p-type GaSb. The relative elevation becomes large with increasing n_i. On the other hand, it is found that C decreases with elevating the quasi-Fermi level, i.e., with decreasing η_p in Eqs. (2.24) and (2.25), if C is calculated with all other parameters fixed. From a viewpoint of the quasi-Fermi level, therefore, the increase of n_i results in the decrease of C. Next, we consider the effect of the tail states on the Auger transition probability. The transition, where the total momentum is not conserved in the presence of randomly distributed impurities and the total energy is conserved, is schematically shown in Figs. 1(b) and 1(c). These figures show the cases for $E_G \gg \Delta_0$ and $E_G < \Delta_0$, respectively. From a view point of the statistical factor Θ_{IF} a small E_3 is favorable for the transitions. From this we find that in the case of $E_G \gg \Delta_0$ the tail states play a dominant role of the effective final states for the transitions. In the case of $E_G \lesssim \Delta_0$, on the other hand, the intraband states play a dominant role.

Based on the above considerations, the contrast between the cases of GaAs and GaSb especially for a low temperature is explained as follows. For GaAs having $E_G \gg \Delta_0$, an increase of the number of the tail states leads to both an increase of the effective final states and the relative elevation of the quasi-Fermi level. These have a positive effect and a neg-

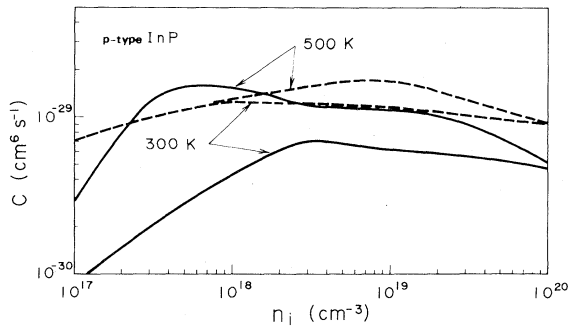

FIG. 7. Auger coefficients C vs n_i at 300 and 500 K on p-type InP for the ps results (solid line) and for the BT results (dashed line).

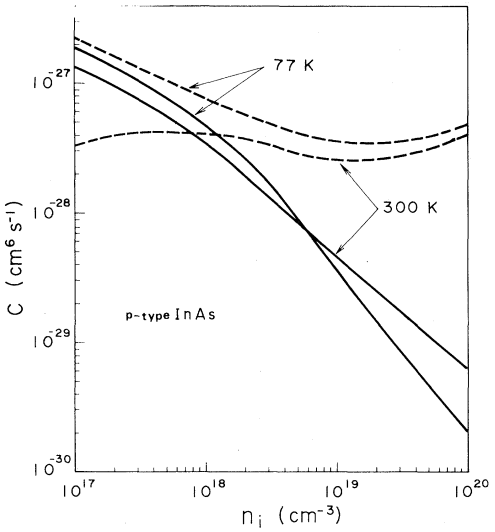

FIG. 8. Auger coefficients vs n_i at 77 and 300 K on p-type InAs for the ps results (solid line) and for the BT results (dashed line).

ative effect, respectively, on AR. The positive effect surpasses the negative effect, resulting in the increase of C with increasing n_i. For GaSb having $E_G \simeq \Delta_0$, where the tail states serve only partly as the effective final states, the above-mentioned negative effect surpasses the positive effect, resulting in the decrease of C with increasing n_i. That the intraband states are also the effective final states means that C for GaSb may contain considerable errors, since the ps theory is useful mainly for description of the tail states. A calculation of the conductivity offers a useful test of the ps theory especially for the intraband states. It is found for p-type GaAs at 300 K that calculated conductivities are considerably smaller than the experimental ones especially at high acceptor concentrations. This may give an explanation of having smaller theoretical values of C than the experimental ones especially for p-type GaSb.

Figures 6—8 show the ps results (solid line) of the Auger coefficients as functions of n_i for two temperatures on p-type materials of GaAs, InP, and InAs. In the figures the BT results (dashed line) are also shown for comparison. It is seen that in gross GaAs, InP, GaSb, and InAs are classified, from a view point of the n_i dependence of C, into two groups according to which of $E_G \gg \Delta_0$ or $E_G \lesssim \Delta_0$ those materials have. At high temperatures the effect of the tail states is not evident for GaAs and InP but is still evident for InAs. In the case of GaSb, a calculation for a high temperature requires consideration of the effect of the indirect band for CB, which lies a little above[25] (~ 0.07 eV) the direct band. The calculation is beyond the scope of this paper.

In conclusion, we have to correctly take into account the effect of the tail states only at low temperatures in the case of $E_G \gg \Delta_0$ and over a wider temperature range in the case of $E_G \lesssim \Delta_0$ for the calculations of the AR rates in a p-type material. In the case of $E_G \gg \Delta_0$ at high temperatures, however, the ps theory and the BT theory give practically the same results in the range of $n_i \gtrsim 10^{18}$ cm^{-3}. As for the acceptor concentration dependence of the Auger coefficient for p-type GaSb, the ps theory gives the shape of a curve similar to the experimental one in contrast to the BT theory. As for p-type GaAs, on the other hand, both theories well explain the experiments.

ACKNOWLEDGMENTS

The author wishes to express his appreciation to Dr. G. Kano, Dr. I. Teramoto, and Dr. H. Mizuno for their constant encouragement.

[1]For review articles, see P. T. Landsberg, Phys. Status Solidi A 41, 457 (1970); A Haug, in *Festkörperprobleme XII, Advances in Solid State Physics,* edited by O. Madelung (Pergamon, Braunschweig, 1972). p. 411; R. Conradt, *ibid.,* p. 449; P. T. Landsberg and M. J. Adams, J. Lumin. 7, 3 (1973).
[2]A. R. Beatie and P. T. Landsberg, Proc. R. Soc. London Ser. A 249, 16 (1959).
[3]M. Takeshima, J. Appl. Phys. 46, 3082 (1975).
[4]L. Huldt, Phys. Status Solidi A 8, 173 (1971).
[5]L. Huldt, Phys. Status Solidi A 24, 221 (1974).
[6]D. Hill and P. T. Landsberg, Proc. R. Soc. London Ser. A 347, 547 (1976).
[7]G. Benz and R. Conradt, Phys. Rev. B 16, 843 (1977).
[8]R. Conradt, Z. Phys. 209, 445 (1968).
[9]M. Takeshima, Phys. Rev. B 23, 771 (1981).
[10]M. Takeshima, Phys. Rev. B 26, 917 (1982).
[11]L. Huldt, Phys. Status Solidi A 33, 607 (1976).
[12]M. Takeshima, Phys. Rev. B 23, 6625 (1981).
[13]M. Takeshima, Phys. Rev. B 25, 5390 (1982).
[14]V. L. Bonch-Bruevich, in *Semiconductors and Semimetals,* edited by R. K. Willardson and A. C. Beer (Academic, New York, 1966), Vol. 1, Chap. 4.
[15]M. Takeshima, Phys. Rev. B 27, 2387 (1983).
[16]M. Takeshima, Phys. Rev. B 26, 3192 (1982).
[17]C. J. Hwang, Phys. Rev. B 2, 4117 (1970).
[18]W. Lochmann, Phys. Status Solidi A 40, 285 (1977).
[19]M. Newberger, in *III-V Semiconducting Compounds* (IFI/Plenum, New York, 1971).
[20]E. O. Kane, in *Semiconductors and Semimetals,* edited by R. K. Willardson and A. C. Beer (Academic, New York, 1966), Vol. 1, Chap. 3.

[21]P. Lawaetz, Phys. Rev. B 4, 3460 (1971).
[22]J. D. Wiley, in *Semiconductors and Semimetals,* edited by R. K. Willardson and A. C. Beer (Academic, New York, 1975), Vol. 10, Chap. 2.
[23]J. Jastrzebski, J. Logowski, H. C. Gatos, and W. Walukiewicz, in *Proceedings of the International Conference on Gallium Arsenide and Related Compounds, 1979,* edited by C. M. Wolfe (The Institute of Physics, Bristol, 1979), p. 437.
[24]A. N. Titkov, G. V. Benemanskaya, B. L. Gelmont, G. N. Iluridthe, and Z. N. Sokolova, J. Lumin. 24/25, 697 (1981).
[25]A. Ya. Vul', L. V. Golubev, T. A. Polyanskaya, and Yu. V. Shmartsev. Fiz. Tekh. Poluprovdn. 3, 301, 786 (1969) [Sov. Phys.—Semicond. 3, 256, 671 (1970)].